Chiang Mai Journal of Science

Chiang Mai J. Sci., 2026; **52(x)**: e2026000
DOI 10.12982/CMJS.2026.000

Detection of Prostate Cancer with Surface Acoustic Wave Biosensors on GO-modified Surface

Suparat Tongpeng, Chayapat Weerapakdee, Soodkhet Pojprapai and Sukanda Jiansirisomboon*
School of Ceramic Engineering, Institute of Engineering, Suranaree University of Technology, Nakhon Ratchasima 30000, Thailand
* Author for corresponding; e-mail address: sukanda.jian@sut.ac.th
ORCID ID: 0000-0001-5015-7370

Received: 29 June 2025 **Revised**: 30 September 2025 **Accepted**: 20 October 2025 **Published**: November 2025
Citation: Tongpeng S., Weerapakdee C., Pojprapai S. and Jiansirisomboon S., Detection of prostate cancer with surface acoustic wave biosensors on GO-modified surface. *Chiang Mai Journal of Science*, 2025; **52(x)**: e2025000. DOI 10.12982/CMJS.2025.000.

GRAPHICAL ABSTRACT

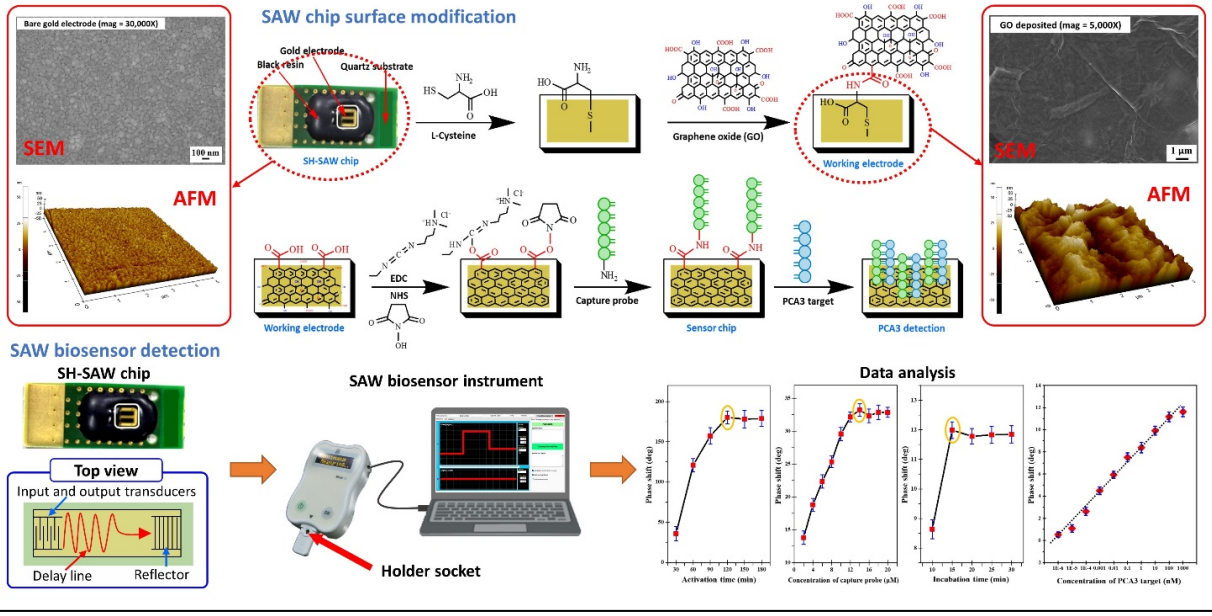

ABSTRACT

Prostate cancer antigen 3 (PCA3) screening has the potential to detect prostate cancer early and assess the efficacy of surgery or radiation therapy. Nanotechnology integration in biosensor development enables effective targeted biomarker detection. Diagnosis of prostate cancer via PCA3 biomarker detection is promising to be much more efficient than with the prostatic-specific antigens currently used. In this study, we developed a GO/PCA3 marker on a surface acoustic wave (SAW) biosensor. The GO-modified SAW biosensor was prepared by conjugating GO onto L-Cysteine on the SAW chip surface. Afterward, the PCA3 capture probe was immobilized on the GO surface, and characterization was performed with XRD, SEM, AFM, and FTIR techniques. This result confirmed the successful deposition of GO, increasing the number of binding sites for interaction between GO and PCA3 capture probe through enhanced sensor surface area. The effects of EDC-NHS activation time, capture probe concentration, and incubation time were optimized. The sensor has a wide linear response that extends from 1.00 fM to 1.00 µM of PCA3 target, and the limit of detection (LOD) is 0.27 nM. These characteristics make the SAW device a promising candidate for various clinical and rapid detection applications.

Keywords: SAW Biosensor, PCA3, prostate cancer, graphene oxide

Chiang Mai J. Sci., 2026; 52(x): e2026000
DOI 10.12982/CMJS.2026.000

1. INTRODUCTION

Prostate cancer (PCa) remains a significant global health challenge, ranking as one of the most commonly diagnosed malignancies among men and contributing substantially to cancer-related morbidity and mortality, with 1.41 million new cases reported in 2020 [1]. Timely identification of PCa is critical for initiating therapy, which can improve patient prognosis, reduce disease progression, and increase survival rates. In PCa diagnostics, prostate cancer antigen 3 (PCA3) is a prostate-specific, long non-coding RNA (lncRNA) that is significantly overexpressed in malignant prostate tissue compared to healthy prostate cells [2, 3]. Unlike traditional biomarkers such as prostate-specific antigen (PSA), which suffers from limited specificity and often results in false positives and unnecessary biopsies, PCA3 exhibits superior diagnostic performance [4]. Clinical investigations have reported a median PCA3 concentration of approximately 31.7 ng/mL in urine samples, with sensitivity and specificity of approximately 87%, highlighting its potential as a reliable diagnostic indicator [5]. Furthermore, detection of low PCA3 levels may indicate early tumorigenesis or disease progression, reinforcing the need for highly sensitive detection technologies.

The integration of biosensor technology with PCA3 detection presents a transformative opportunity to enhance prostate cancer screening methodologies, offering a non-invasive, accurate, and patient-centric alternative to conventional diagnostic procedures, particularly within the framework of point-of-care testing (POCT) [6]. This approach could reduce the reliance on invasive procedures such as prostate biopsies, which are often performed unnecessarily on individuals with low cancer risk [7]. Among the various biosensor platforms, surface acoustic wave (SAW)-based biosensors have garnered considerable attention due to their capacity to detect physical, chemical, and biological analytes with high precision and sensitivity. SAW biosensors operate based on the propagation of acoustic waves along the surface of piezoelectric substrates, where interactions with target molecules induce measurable changes in wave characteristics such as frequency, amplitude, or phase [8-10]. Moreover, the surface-sensitive nature of their acoustic modes, combined with high operating frequencies, confers SAW biosensors with enhanced mass sensitivity, underscoring their performance [11, 12]. SAW biosensors offer several advantages that make them suitable for POCT applications, including rapid response times, operation at ambient temperatures, high sensitivity, low manufacturing costs, simplicity of the test procedure, and excellent stability under diverse environmental conditions [13]. Consequently, the development of SAW biosensors tailored for PCA3 detection within POCT platforms represents a significant advancement toward more efficient, reliable, and accessible prostate cancer diagnostics.

Despite these promising developments, detecting PCA3 in complex biological fluids remains technically challenging, primarily due to their low endogenous concentrations, molecular instability, and interference from biological matrices [14]. Therefore, enhancing the sensitivity, specificity, and signal amplification capabilities of SAW biosensors is essential to ensure reliable detection. A widely adopted strategy to achieve this involves modifying the sensor surface with functional nanomaterials to improve analytical performance [15]. Graphene oxide (GO), a two-dimensional carbon-based nanomaterial, has emerged as an ideal candidate for enhancing surface sensor chips due to its unique physicochemical properties [16]. GO exhibits high electrical conductivity, a high surface-to-volume ratio, superior mechanical strength, and excellent biocompatibility, making it particularly well-suited for biosensing applications [17]. The abundant oxygen-containing functional groups present on GO facilitate the efficient immobilization of biorecognition elements, such as single-stranded DNA (ssDNA), RNA probes, aptamers, or antibodies, thereby enhancing probe density, target capture efficiency, and overall sensor sensitivity [18]. Furthermore, the GO-based biosensors suggest their applicability extends beyond PCA3 detection to encompass a broad range of oncogenic biomarkers for early cancer diagnosis and monitoring.

In this study, the researchers aimed to optimize the stability and dispersibility of GO suspension, as well as the immobilization of the capture probe on the surface of a shear horizontal surface acoustic wave (SH-SAW) sensor chip [19-21]. This was achieved through the chemical functionalization of GO with carboxyl (COOH) and hydroxyl (OH) groups, enhancing its chemical reactivity and the binding efficiency of the capture probe [22]. The SH-SAW sensor chip was fabricated using a layer-by-layer assembly of L-cysteine, GO, and EDC-NHS, which improved the capture probe immobilization efficiency. Subsequently, an amine-functionalized capture probe was immobilized onto the GO-modified surface. The detection of the PCA3 target was quantified by monitoring phase shift ($\Delta\varphi$) signals, providing real-time information on each step of the sensor chip fabrication.

2. MATERIALS AND METHODS

2.1 Materials and characterization

The capture probe (NH_2-$(CH_2)_{12}$-5'-TTTTTTTCCCAGGGATCTCTGTGCTTCC-3', 100 µM, M.W. 8478.54 g/mol) and PCA3 target (5'-GGAAGCACAGAGATCCCTGGG-3', 100 µM, M.W. 6505.10 g/mol) were purchased from U2Bio (Thailand) Co., Ltd. Ethanol (99.9%), 1-ethyl-3-(3-dimethylaminopropyl) carbodiimide (EDC), N-hydroxysuccinimide (NHS), L-cysteine hydrochloride monohydrate (L-Cys) were purchased from Sigma-Aldrich. For phosphate buffer saline (PBS, 1X, pH 7.4), sodium chloride (NaCl, 8.01 g),

potassium chloride (KCl, 0.20 g), sodium phosphate monobasic dihydrate ($NaH_2PO_4.2H_2O$, 1.78 g), and potassium phosphate monobasic (KH_2PO_4, 0.24 g) were purchased from Merck. Graphene oxide (GO) solution was acquired 1.20 g/100 mL from Haydale Technologies (Thailand) Company Limited. The GO was diluted to 0.10 mg/mL in deionized (DI) water using an ultrasonic probe.

For characterization, the morphologies were examined field emission scanning electron microscopy (FE-SEM, Carl Zeiss, Aurica, Germany) combined with energy dispersive X-ray spectroscopy (EDS). Contact mode atomic force microscopy (AFM, XE-120 Park Systems, scan frequency 0.2 Hz, 512 lines) was used to scan $5 \times 5\ \mu m^2$ sample areas. AFM images were analyzed using XEI software (Park Systems) to extract the roughness information from the sample surfaces. The X-ray diffraction (XRD) patterns for different samples were recorded using a D8 Advance (Bruker, Germany) diffractometer using Cu-Kα radiation source (λ = 1.5406 Å) at a scanning speed of 0.10°/min in the 5-80° 2θ range. Chemical functional groups investigated by Fourier transform infrared spectroscopy (FTIR, Bruker Tensor 27-Hyperion 2000) spectra using a Perkin Elmer spectrum GX. The spectra were measured in the specular reflectance mode in the wavenumber range of 4000-400 cm^{-1}.

2.2 Modification of GO and immobilization of capture probe

The process of preparing the detection chip consisted of six steps, as shown in **Figure 1**. (1) The gold surface of the sensor chip was cleaned and sequentially ultrasonicated in DI water, anhydrous ethanol, and DI water for 20 minutes to remove any adsorbed surface substances. (2) The cleaned chip was dried with nitrogen and incubated with 0.10 mM L-Cys for 2 hours at room temperature. The chip was rinsed with DI water and dried with nitrogen. (3) The L-Cys surface of the sensor chip was covered with the diluted GO suspension overnight at room temperature. After deposition, washing, and drying, the GO-modified chip was obtained. (4) The carboxyl groups of GO on the chip surface were activated with a mixture solution of EDC and NHS (1:1 of 0.10 mM EDC: 0.10 mM NHS). The chip was rinsed with DI water and dried with nitrogen. (5) The capture probe preparation with different concentrations (2 - 20 μM) was diluted in PBS buffer. An appropriate concentration of capture probe solution was dropped on the chip and immobilized in the dark overnight at room temperature. After being carefully rinsed with PBS buffer to remove excess capture probe and dried with nitrogen, the sensor chip was obtained. (6) 1 μM PCA3 target in PBS buffer was injected on the surface sensor chip to hybridize with the capture probe at room temperature.

2.3 SAW biosensor measurement

SAW biosensor devices were used for all the prostate cancer sensing experiments (**Figure 2**). The sensor chip was designed to excite a shear-horizontal SAW (SH-SAW) on a quartz substrate with a center frequency of 250 MHz [23-25]. On the chip, SAW is excited at an input interdigital transducer (IDT). Then it propagates back and forth between a reflector and an output transducer over a delay line that was used as a sensing region, as shown in **Figure 2(c)**. Afterwards, the wave is converted back at another IDT into an electrical signal. Input and output signals are transformed, resulting signal of phase shift ($\Delta\varphi$), which can then be correlated to the corresponding mass and mechanical properties in the fluid contacting the

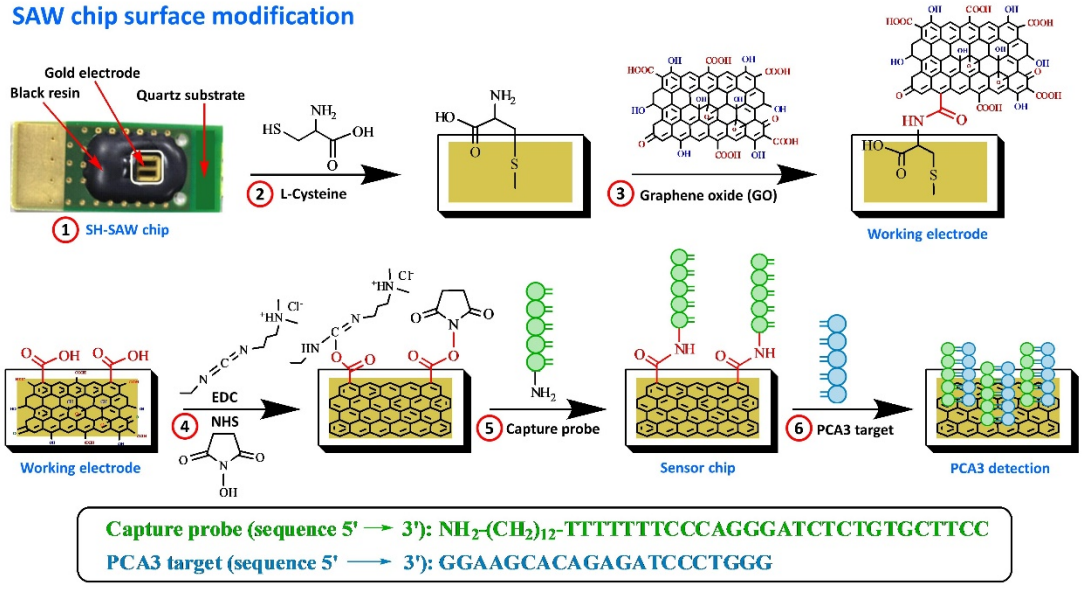

Figure 1 Schematic chemical structure diagram of SH-SAW chip based on GO-modified for prostate cancer detection.

Chiang Mai J. Sci., 2026; 52(x): e2026000
DOI 10.12982/CMJS.2026.000

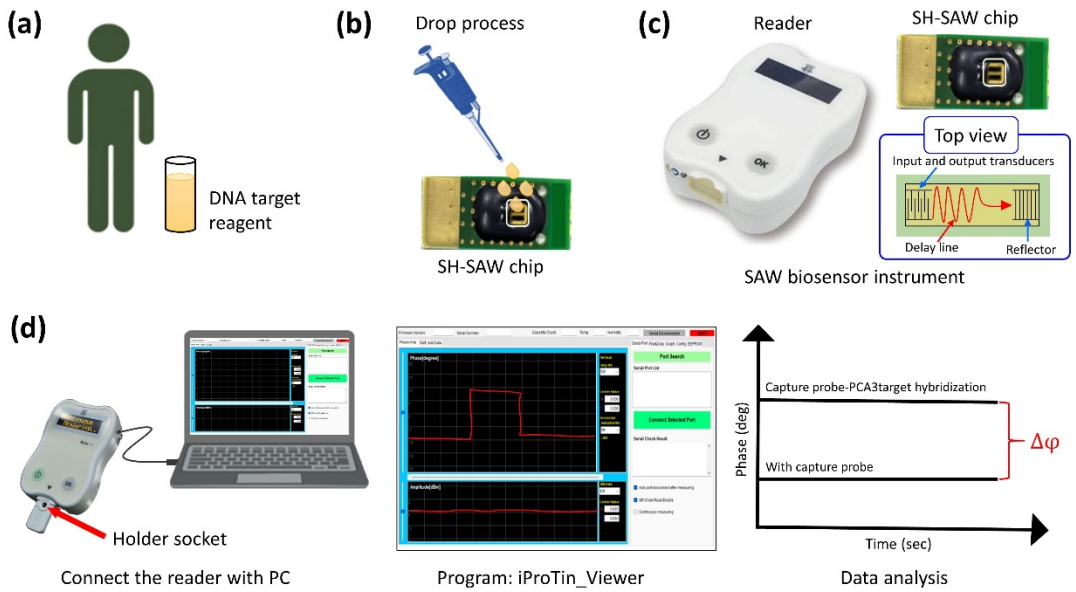

Figure 2 Photographs of SAW biosensor instrument (a) target sample, (b) drop process, (c) SAW biosensor portable and SH-SAW chip, and (d) SAW instrument setup, software, and phase signal.

sensing surface [26]. Phase measurement was recorded before and after the injection of sample into the sensor's holder socket using a micropipette (**Figure 2(d)**). Target hybridization was monitored in real-time by recording the phase shift, and measurements were repeated three times. The following optimization studies were conducted: activation time, concentrations of capture probe, incubation time, and concentrations of PCA3 target (The PCA3 target preparation with different concentrations (1 fM - 1 μM) was diluted in PBS buffer).

The selectivity of PCA3 detection in PBS buffer was evaluated using negative control experiments. These experiments employed several analytes, namely epidermal growth factor receptor (EGFR, 1 nM), distal-less homeobox 1 (DLX1, 1 nM), and blank. To measure the phase shift of negative control, 5 μL of each analyte was injected onto SAW sensor chip under similar experimental conditions.

3. RESULTS AND DISCUSSION

FE-SEM and AFM were employed to characterize the morphology of the bare gold electrode and GO deposited on the electrode surfaces of the SH-SAW sensor chip, as shown in **Figure 3**. FE-SEM and AFM images of the bare gold electrode reveal a characteristic grainy surface structure typical of gold nanoparticles. After GO deposition, the electrode surface exhibited a thin, wrinkled, sheet-like morphology with discernible edges. **Figure 3(a)** shows that the GO formed a homogeneous composition of overlapping flakes, uniformly covering the gold surface of the SH-SAW chip. This uniform coverage extended across large surface areas. Further characterization using AFM confirmed changes in surface topography, as presented in **Figure 3(b)**. AFM images show the tapping mode AFM measurements were performed on bare gold electrode and after the deposition of GO. At the GO deposited, the binding of a large GO causes a noticeable increase in grain sizes. Two-dimensional AFM roughness analysis provided quantitative evidence of GO surface. The root mean square roughness (R_q) increased significantly from 1.419 nm (bare gold) to 8.547 nm following GO modification, indicating successful surface modification.

Figure 4(a) displays the XRD patterns of the individual layers of the SH-SAW chips, demonstrating a similar pattern with a major peak at 2θ = 38.2° in samples ① - ④. This peak corresponds to the (111) plane of gold (Au) and correlates to the standard reference data (JCPDS 04-0784), confirming the presence of a gold layer on the sensor surface. **Figure 4(b)** presents the XRD patterns in the 2θ range of 5° to 35°. A major peak observed at 2θ = 10.6° corresponds to the (001) plane of graphene oxide in samples ② - ④. This observation confirms the successful oxidation of graphite into graphene oxide. Simultaneously, the minor peak at 2θ = 26.6°, associated with the (002) plane of pristine graphite, as supported by the standard reference (JCPDS 26-1079). The leftward shift of the diffraction peak reflects an increase in interlayer spacing, providing further evidence of the effective oxidation process and the successful formation of graphene oxide.

The FTIR spectrum of modified surface is shown in **Figure 4(c)** confirming the presence of chemical bonds present in immobilized matrix due to surface modification steps. The sample ① of L-Cys layer shows peaks at 3053 cm^{-1}, 1710 cm^{-1}, and 1062 cm^{-1}, which

Chiang Mai J. Sci., 2026; 52(x): e2026000
DOI 10.12982/CMJS.2026.000

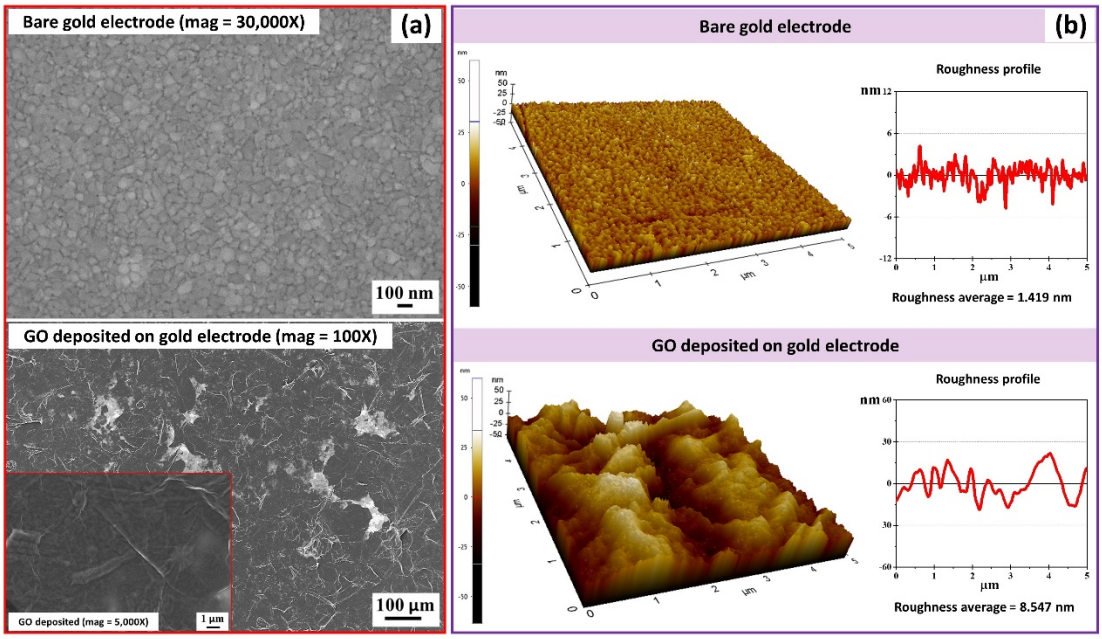

Figure 3 Bare gold electrode and GO deposited on the surface of gold electrode (a) FE-SEM images and (b) AFM topography and roughness profile.

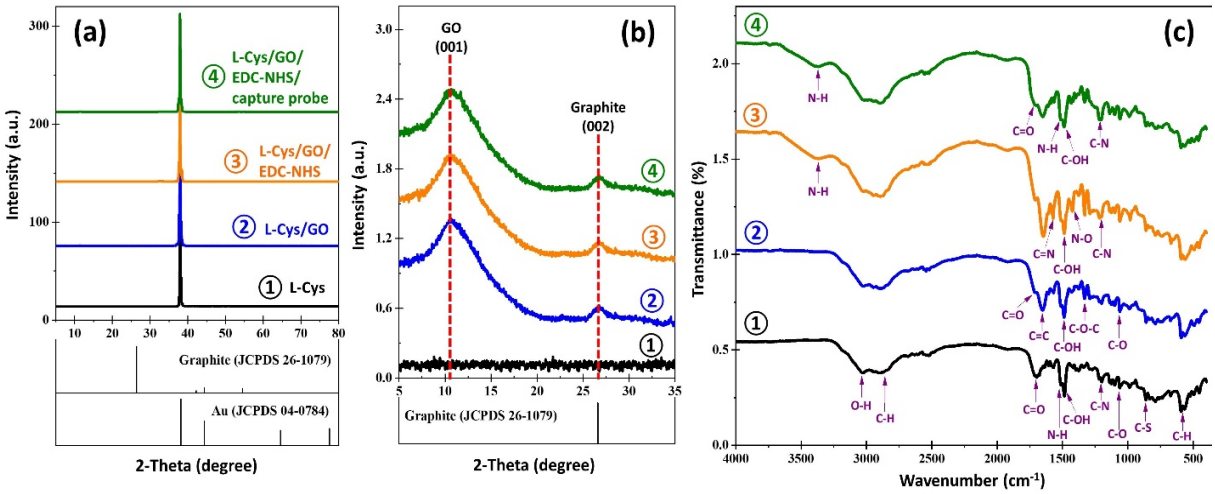

Figure 4 XRD patterns of SH-SAW chips functionalized for each layer (a) 2-theta ranges of 5° – 80° and (b) 2-theta ranges of 5° – 35°. (c) FTIR spectra of SH-SAW chip functionalized for each layer.

are assigned to the OH (hydroxyl), C=O, and C–O stretching vibrations of carboxylic group, respectively. Whereas, the peaks at 1517 cm^{-1}, 1205 cm^{-1}, 865 cm^{-1}, and 594 cm^{-1} corresponds to the N–H (bending), C–N (bending), C–S (bending), and C–H (bending) band, respectively. The sample ② of graphene oxide coated on L-Cys layer exhibited several absorption bands, indicating the presence of aromatic double bonds and oxygen-containing functional groups, thereby affirming the success of the GO deposition. The GO shows strong peaks at 1712 cm^{-1} and 1652 cm^{-1} which are assigned to the C=O vibrations carboxylic group and C=C (aromatic) stretching vibrations of aromatic. Additionally, the FTIR bands observed at 2893 cm^{-1} is attributed to the asymmetric and symmetric stretching of C–H in GO. A broad peak spanning the range between 3020 cm^{-1} emerged, which can be ascribed to the OH stretching vibrations arising from hydroxyl groups and carboxylic group. The GO spectrum also manifests bands corresponding to C–OH at 1490 cm^{-1}, C–O–C at 1334 cm^{-1}, and C–O at 1064 cm^{-1} functionalities present in carboxylic acid and carbonyl moieties. When EDC-NHS activated on GO layer in sample ③, spectrum shows intense peaks at 1427 cm^{-1}, 1571 cm^{-1}, and 3375 cm^{-1}, which can be attributed to the N–O stretch, C=N stretch, and N–H stretch as well as C–N (1202 cm^{-1}) stretch in NHS esters. After coating capture probe at sample ④, the deconvolution peak of C–N in the amide bond was

Chiang Mai J. Sci., 2026; 52(x): e2026000
DOI 10.12982/CMJS.2026.000

enhanced while the N–O peak decreased. This clearly shows the emergence of the C–N peak corresponding to the amine of the capture probe coupling with carboxyl groups on the GO. Hence, FTIR analysis confirmed the coordination of all the immobilized materials on GO. The results above indicate the successful GO and biomarker coating onto the gold sensor chip surface.

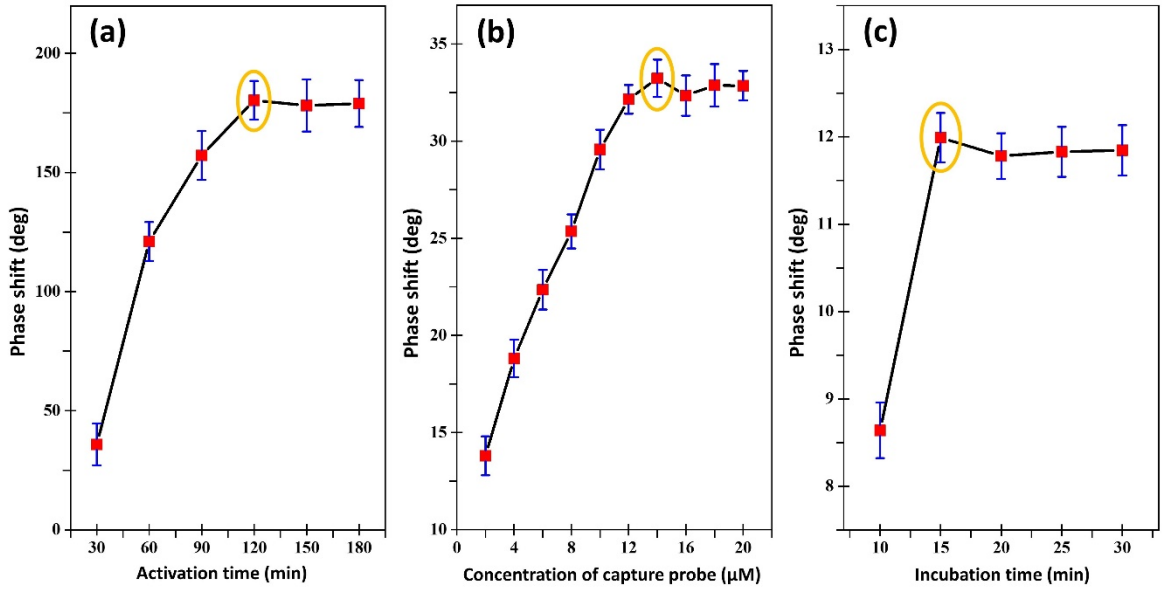

Figure 5 Optimization studies (a) effect of different activation time of EDC-NHS (30-180 min), (b) effect of different concentrations of capture probe (2-20 μM), and (c) effect of different incubation time after hybridization with the PCA3 target at 1 μM (10-30 min). The error bars indicate the standard deviations of three independent experiments.

3.1 Optimization Studies

To detect the PCA3 target using the SAW biosensor. Acoustic waves were generated by the input interdigital transducer (IDT) and detected at the output IDT through a gold electrode. Adsorption of materials onto the gold surface resulted in changes in viscosity and weight, which in turn caused a delay in the SAW propagation. The phase shift of the SH-SAW biosensor was thus observed for the mass-change in the working electrode area. Additionally, the SH-SAW chip monitored the construction of the activation time of EDC-NHS on the GO deposit surface, capture probe immobilization, and the detection of PCA3 target by the phase shift, as shown in **Figure 5**. The real-time detection in the phase signal correlated with the increase in the chemical molecules captured. Initially, the effect of carboxylic group activation using EDC-NHS was investigated to determine the optimal conditions for effective cross-linking and subsequent capture probe immobilization. **Figure 5(a)** illustrates the phase shift as a function of activation time with EDC-NHS, ranging from 30 to 180 minutes. The results show that the phase shift stabilized at 120 minutes, indicating this as the optimal activation time. **Figure 5(b)** depicts the phase shift of the capture probe within the concentration range of 2 to 20 μM. The results indicate that the phase shift begins to stabilize at a probe concentration of 12 μM, suggesting that a sufficient amount of capture probe has been immobilized on the electrode surface. Therefore, a concentration of 14 μM was identified as optimal, as it yielded the maximum phase shift, and was subsequently employed for sensor chip preparation.

The sensitivity of the SAW biosensing platform for PCA3 system quantification was investigated by recording the phase shift resulting from the hybridization of the PCA3 target with the capture probe at a concentration of 14 μM. Additionally, the recognition time required for the capture probe to bind the target molecule was investigated by incubating the sensor chip with 1 μM of the PCA3 target over varying time intervals (10-30 minutes). **Figure 5(c)** presents the phase shift responses corresponding to different incubation times. Analysis of the phase shift indicated that the incubation time stabilized at 15 minutes. Therefore, an incubation period of 15 minutes was selected for PCA3 target hybridization, as it yielded the optimal signal response. The sensor chip modification exhibited the highest binding response to the PCA3 target, as indicated by consistent phase shift values of approximately 11.98°. These results suggest that covalent binding via EDC-NHS activation, achieved through amine coupling on the carboxylated surface, facilitates site-specific immobilization of the capture probe. This covalent attachment helps preserve the probe's functional conformation and reduces denaturation, thereby maintaining the availability of

Chiang Mai J. Sci., 2026; 52(x): e2026000
DOI 10.12982/CMJS.2026.000

target-binding sites. Furthermore, the presence of carboxylic moieties on the electrode surface offers improved anchoring sites for biomarker immobilization through CO–NH linkages. The working electrode layer also enables efficient and well-dispersed immobilization of a large quantity of capture probe within the GO surface.

limit of detection (LOD) was calculated using the following equation:

$$LOD = \frac{3\sigma}{S}$$

where σ is the standard deviation and S is the slope of a calibration curve [27]. Based on this calculation, the developed sensor exhibited an LOD = 0.27 nM, corresponding to 1.76 ng/mL. A correlation coefficient

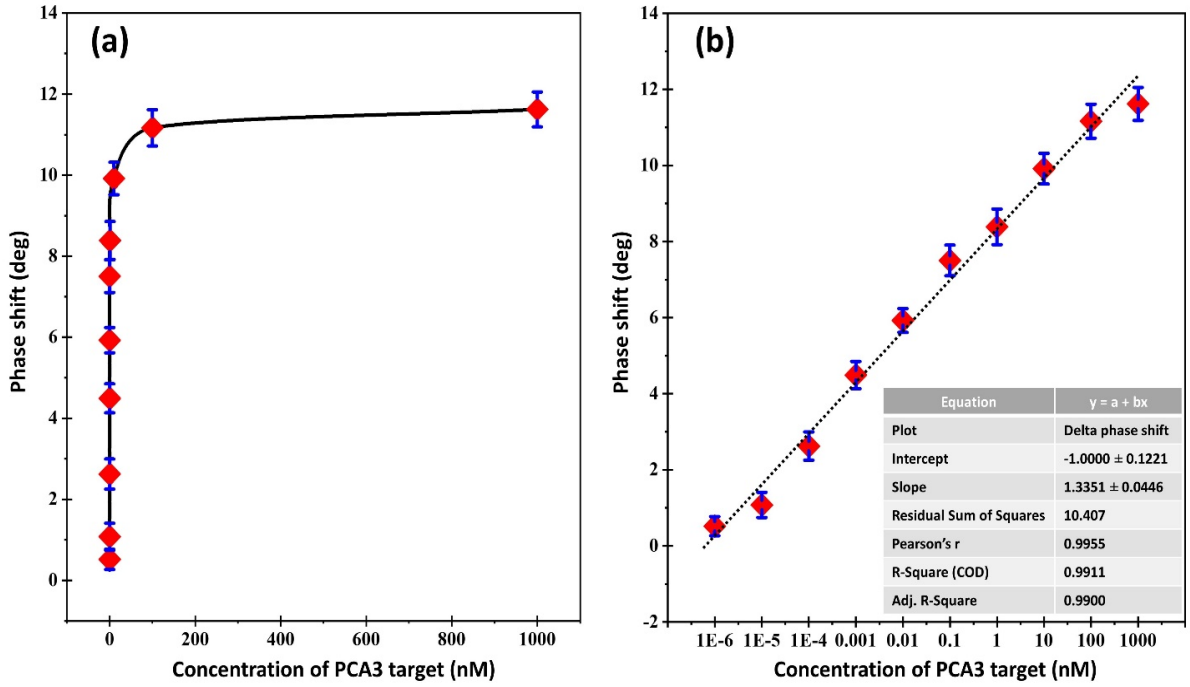

Figure 6 Effect of PCA3 target concentration (a) phase shift of PCA3 target incubated with different concentrations from 1 fM to 1 µM and (b) calibration plot between phase shift and logarithm of linear PCA3 target concentrations. The error bars indicate the standard deviations of three independent experiments.

3.2 GO-SAW biosensor performance for PCA3 detection

Under optimized experimental conditions, the SH-SAW sensor chip was fabricated by depositing GO, followed by activation using an EDC-NHS solution for 120 minutes. Subsequently, a capture probe was immobilized at a concentration of 14 µM. After that, the PCA3 target was injected at varying concentrations from 1 fM to 1 µM. Phase shift measurements were recorded 15 minutes after the initial injection, followed by rinsing with PBS buffer to remove unbound molecules. **Figure 6(a)** presents the phase shift as a function of PCA3 target concentration within the test range. The calibration curve demonstrates a linear relationship between the phase shift and the logarithm of the PCA3 target concentration, as shown in **Figure 6(b)**. The results reveal a gradual increase in phase shift with increasing PCA3 target concentration, indicating effective target recognition and binding. A slope of 1.3351 was obtained for the calibration curve, with a corresponding standard deviation of 0.1221. The (R^2 = 0.99) was obtained, indicating a high degree of linearity within the tested concentration range. These results demonstrate that the GO-modified SH-SAW sensing chip exhibits excellent performance in terms of both quantitative analysis and specificity. The improved detection ability can be attributed to the efficient immobilization of biomolecules on the GO surface, which enhances the interaction between the capture probe and the PCA3 target analyte. The increased surface area and the presence of functional groups on GO facilitate more effective hybridization, resulting in a stronger and more reliable sensor response. Furthermore, the low detection limit was achieved in a significantly shorter time compared to conventional detection methods, such as biopsy. Therefore, the GO-modified SH-SAW system shows strong potential for development as a point-of-care diagnostic tool for clinical applications. Additionally, we compared the sensitivity of our approach with that of previously reported SAW-based methods and other techniques with various surface modification strategies for signal

Chiang Mai J. Sci., 2026; 52(x): e2026000
DOI 10.12982/CMJS.2026.000

Table 1 The performance characteristics of prostate cancer detection with other methods previously reported.

Method	Biomarker	Linear range	Detection limit (nM)	Reference
Electrochemical (DPV)	Prostate-specific membrane antigen	0-5 ng/mL	0.47 ng/mL	[28]
Fluorescent (IFE)	Sarcosine	0.5-5 μM	0.12 μM	[29]
Colorimetric (POCT)	Citrate	0.5-1000 μM	0.1 μM	[30]
Electrochemical	PCA3	0.1 – 10 μg/mL	2.2 ng/mL	[31]
Electrochemical	PCA3	0.1 ng/mL – 1 μg/mL	0.4 nM	[32]
SAW biosensor	PCA3	1 fM – 1 μM	0.27 nM	This work

amplification. The comparative results are summarized in **Table 1**.

To evaluate the specificity of the SAW biosensor, negative control experiments were performed using non-target biomolecules, including EGFR (1 nM), DLX1 (1 nM), and a blank sample, as shown in **Figure 7**. The sensor response to these negative controls was negligible and comparable to that of the blank. It was significantly lower than the response observed for PCA3 at its lowest detectable concentration (1 fM). These findings confirm the excellent selectivity of the biosensor, which is attributable to the high affinity and specificity of the capture probe for the PCA3 target sequence.

the PCA3 target, leading to improved phase response and enhanced biosensor performance. SEM and AFM analyses confirmed the successful loading of GO particles onto the surface of the SH-SAW chip, revealing a substantial increase in surface area. Furthermore, FT-IR spectroscopy results corroborated the successful GO treatment, indicating the presence of carboxylic moieties. These improved surface properties are highly advantageous for efficient biomarker immobilization and specific hybridization with a complementary PCA3 target. The key point of this study is the detection of PCA3 in PBS buffer solutions in a wide concentration range from 1 fM to 1 μM. This wide concentration range exhibited a linear calibration, with a remarkable limit

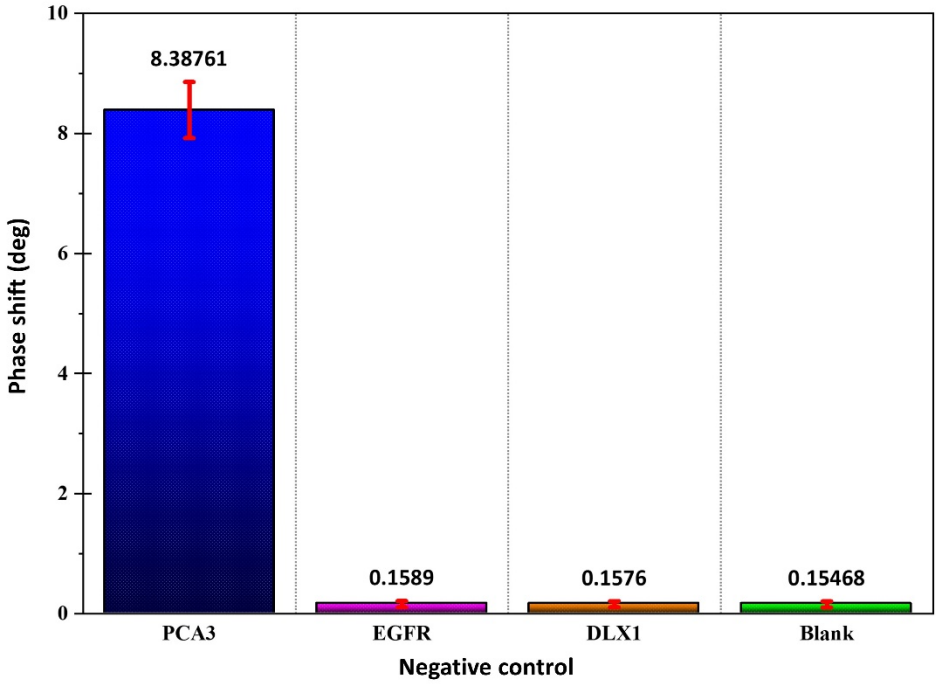

Figure 7 Comparing its phase shift signals to 1 nM of negative control substances such as EGFR, DLX1, and blank. The error bars represent the standard deviation of three independently fabricated sensors.

4. CONCLUSIONS

Graphene oxide (GO) nanoparticles were successfully deposited onto the SH-SAW chip by the drop method. The GO structures significantly enhance biomarker binding and more effective interactions with

of detection (LOD) of 0.27 nM. The ability to detect PCA3 at such low concentrations is critically important for the prospective implementation of this method in the analysis of real urine samples from prostate cancer patients. The excellent selectivity observed is attributed

to the high hybridization efficiency of the capture probe with its specific PCA3 target. The demonstrated high sensitivity and stability of this platform present a promising solution for point-of-care diagnosis of prostate cancer in diverse clinical applications, with potential applicability extending to the analysis of other cancer-related biomolecules.

ACKNOWLEDGEMENTS

This research was supported by Suranaree University of Technology (SUT) and by Office of the Higher Education Commission under NRU Project of Thailand for all facilities and financial supports. The figures in this article were created using Adobe Illustrator, Origin, ChemDraw, and Microsoft PowerPoint.

CONFLICT OF INTEREST STATEMENT

The authors declare that they hold no competing interests.

REFERENCES

[1] Wang L., Lu B., He M., Wang Y., Wang Z. and Du L., Prostate cancer incidence and mortality: Global status and temporal trends in 89 countries from 2000 to 2019. *Frontiers in Public Health*, 2022; **10**: 811044. DOI 10.3389/fpubh.2022.811044.

[2] Takita S., Nabok A., Lishchuk A., Mussa M.H. and Smith D., Detection of prostate cancer biomarker PCA3 with electrochemical apta-sensor. *Engineering Proceedings*, 2022; **16**: 8. DOI 10.3390/IECB2022-12257.

[3] Lemos A.E.G., da Rocha Matos A. and Ferreira L.B., The long non-coding RNA PCA3: An update of its functions and clinical applications as a biomarker in prostate cancer. *Oncotarget*, 2019; **10**: 6589. DOI 10.18632/oncotarget.27284.

[4] Schilling D., De Reijke T., Tombal B., De La Taille A., Hennenlotter J. and Stenzl A., The prostate cancer gene 3 assay: Indications for use in clinical practice. *BJU International*, 2010; **105**: 452-455. DOI 10.1111/j.1464-410X.2009.09085.x.

[5] Ramos C.G., Valdevenito R., Vergara I., Anabalon P., Sanchez C. and Fulla J., PCA3 sensitivity and specificity for prostate cancer detection in patients with abnormal PSA and/or suspicious digital rectal examination. First Latin American experience. *Urologic Oncology*, 2013; **31**: 1522-1526. DOI 10.1016/j.urolonc.2012.05.002.

[6] Lino C., Barrias S., Chaves R., Adega F., Martins-Lopes P. and Fernandes J., Biosensors as diagnostic tools in clinical applications. *Biochimica et Biophysica Acta (BBA)-Reviews on Cancer*, 2022; **1877**: 188726. DOI 10.1016/j.bbcan.2022.188726.

[7] Broomfield J., Kalofonou M., Bevan C.L. and Georgiou P., Recent electrochemical advancements for liquid-biopsy nucleic acid detection for point-of-care prostate cancer diagnostics and prognostics. *Biosensors*, 2024; **14**: 443. DOI 10.3390/bios14090443.

[8] Gronewold T.M., Surface acoustic wave sensors in the bioanalytical field: Recent trends and challenges. Analytica Chimica Acta, 2007; **603**: 119-128. DOI 10.1016/j.aca.2007.09.056.

[9] Huang Y., Das P.K. and Bhethanabotla V.R., Surface acoustic waves in biosensing applications. Sensors and Actuators Reports, 2021; 3: 100041. DOI 10.1016/j.snr.2021.100041.

[10] Fogel R., Limson J. and Seshia A.A., Acoustic biosensors. *Essays in Biochemistry*, 2016; **60**: 101-110. DOI 10.1042/EBC20150011.

[11] Ramaraj S.G., Alrebh A., Elamaran D., Zhou H., Huang K., Almansoori M., et al., Surface acoustic wave gas Sensors: Recent developments and their role in sensing technology. *Materials Science and Engineering: B*, 2025; **317**: 118157. DOI 10.1016/j.mseb.2025.118157.

[12] Aleixandre M. and Horrillo M.C., Recent advances in SAW sensors for detection of cancer biomarkers. Biosensors, 2025; 15: 88. DOI 10.3390/bios15020088.

[13] Horiguchi Y., Miyachi S. and Nagasaki Y., High-performance surface acoustic wave immunosensing system on a PEG/aptamer hybridized surface. *Langmuir*, 2013; **29**: 7369-7376. DOI 10.1021/la304548m.

[14] Zida S.I., Lin Y.D. and Khung Y.L., Current trends on surface acoustic wave biosensors. *Advanced Materials Technologies*, 2021; **6**: 2001018. DOI 10.1002/admt.202001018.

[15] Abdelwahab S.I., Taha M.M.E., Sahli K.A., Alqhtani H.A.S., Farasani A., Khamjan N.A., et al., Graphene-based biosensors for PSA. *Clinica Chimica Acta*, 2025; **576**: 120406. DOI 10.1016/j.cca.2025.120406.

[16] Sutam S., Inyawilert K., Punginsang M., Siriwalai M., Wisitsoraat A., Tuantranont A., et al., Highly selective NO_2 sensors based on electrolytically exfoliated graphene/flame-made WO_3 composite films. *Chiang Mai Journal of Science*, 2023; **50**: e2023067. DOI 10.12982/CMJS.2023.067.

[17] Xuan W., He M., Meng N., He X., Wang W., Chen J., et al., Fast response and high sensitivity ZnO/glass surface acoustic wave humidity sensors using graphene oxide sensing layer. *Scientific Reports*, 2014; **4**: 7206. DOI 10.1038/srep07206.

[18] Baig N. and Saleh T.A., Electrodes modified with 3D graphene composites: A review on methods for preparation, properties and sensing applications. *Microchimica Acta*, 2018; **185**: 1-21. DOI 10.1007/s00604-018-2809-3.

[19] Cheng C.-H., Yatsuda H., Goto M., Kondoh J., Liu S.-H. and Wang R.Y., Application of shear horizontal surface acoustic wave (SH-SAW) immunosensor in Point-of-Care diagnosis. *Biosensors*, 2023; **13**: 605. DOI 10.3390/bios13060605.

[20] Ji J., Pang Y., Li D., Huang Z., Zhang Z., Xue N., et al., An aptamer-based shear horizontal surface acoustic wave biosensor with a CVD-grown single-layered graphene film for high-sensitivity detection of a label-free endotoxin. *Microsystems & Nanoengineering*, 2020; **6**: 4. DOI 10.1038/s41378-019-0118-6.

[21] Rocha-Gaso M.-I., March-Iborra C., Montoya-Baides Á. and Arnau-Vives A., Surface generated acoustic wave biosensors for the detection of pathogens: A review. *Sensors*, 2009; **9**: 5740-5769. DOI 10.3390/s90705740.

[22] Liu L., Zhang M., Huang Z., Cheng W., Meng Y., Wang H., et al., Preparation of magnetic graphene oxide and its application in the detection of Salmonella in chicken. *Chiang Mai Journal of Science*, 2021; **48**: 1524-1537.

[23] Peng Y.-C., Cheng C.-H., Yatsuda H., Liu S.-H., Liu S.-J., Kogai T., et al., A novel rapid test to detect Anti-SARS-CoV-2 N protein IgG based on shear horizontal surface acoustic wave (SH-SAW). *Diagnostics*, 2021; **11**: 1838. DOI 10.3390/diagnostics11101838.

[24] Toma K., Miki D., Kishikawa C., Yoshimura N., Miyajima K., Arakawa T., et al., Repetitive immunoassay with a surface acoustic wave device and a highly stable protein monolayer for on-site monitoring of airborne dust mite allergens. *Analytical Chemistry*, 2015; **87**: 10470-10474. DOI 10.1021/acs.analchem.5b02594.

[25] Mujahid A. and Dickert F.L., Surface acoustic wave (SAW) for chemical sensing applications of recognition layers. *Sensors*, 2017; **17**: 2716. DOI 10.3390/s17122716.

[26] Turbé V., Gray E.R., Lawson V.E., Nastouli E., Brookes J.C., Weiss R.A., et al., Towards an ultra-rapid smartphone-connected test for infectious diseases. *Scientific Reports*, 2017; **7**: 11971. DOI 10.1038/s41598-017-11887-6.

[27] Guider R., Gandolfi D., Chalyan T., Pasquardini L., Samusenko A., Pederzolli C., et al., Sensitivity and limit of detection of biosensors based on ring resonators. *Sensing and Bio-sensing Research*, 2015; **6**: 99-102. DOI 10.1016/j.sbsr.2015.08.002.

[28] Kabay G., Yin Y., Singh C.K., Ahmad N., Gunasekaran S. and Mutlu M., Disposable electrochemical immunosensor for prostate cancer detection. *Sensors and Actuators B: Chemical*, 2022; **360**: 131667. DOI 10.1016/j.snb.2022.131667.

[29] Lin X., Tian M., Cao C., Shu T., Wen Y., Su L., et al., Using bimetallic Au/Cu nanoplatelets for construction of facile and label-free inner filter effect-based photoluminescence sensing platform for sarcosine detection. *Analytica Chimica Acta*, 2022; **1192**: 339331. DOI 10.1016/j.aca.2021.339331.

[30] Abarghoei S., Fakhri N., Borghei Y.S., Hosseini M. and Ganjali M.R., A colorimetric paper sensor for citrate as biomarker for early stage detection of prostate cancer based on peroxidase-like activity of cysteine-capped gold nanoclusters. *Spectrochimica Acta Part A: Molecular and Biomolecular Spectroscopy*, 2019; **210**: 251-259. DOI 10.1016/j.saa.2018.11.026.

[31] Mokni M., Tlili A., Khalij Y., Attia G., Zerrouki C., Hmida W., et al., Designing a simple electrochemical genosensor for the detection of urinary PCA3, a prostate cancer biomarker. *Micromachines*, 2024; **15**: 602. DOI 10.3390/mi15050602.

[32] Nabok A., Abu-Ali H., Takita S. and Smith D.P., Electrochemical detection of prostate cancer biomarker PCA3 using specific RNA-based aptamer labelled with ferrocene. *Chemosensors*, 2021; **9**: 59. DOI 10.3390/chemosensors9040059.